# Glyoxal-induced disruption of tumor cell progression in breast cancer

PU RONG[1,2*], LI YANCHU[3*], GUO NIANCHUN[2], LI QI[2] and LI XIANYONG[1,2]

Departments of [1]Oncology and [2]Research, Chengdu Fuxing Hospital, Chengdu, Sichuan 610037; [3]Department of Head and Neck Oncology, West China Hospital of Sichuan University, Chengdu, Sichuan 610041, P.R. China

Received December 16, 2020; Accepted October 8, 2021

DOI: 10.3892/mco.2023.2622

**Abstract.** Breast cancer is the most common malignant tumor in women and remains a major global challenge, with ~1.4 million cases per year, worldwide. Numerous studies have shown that changes in cell metabolism are associated with the regulation of tumor progression. In the present study, the anti-cancer properties of glyoxal (GO), which is the smallest dialdehyde formed in the oxidation-reduction reaction and involved in electron transfer and energy metabolism, in breast cancer was investigated. The biological functions and molecular mechanisms of GO were investigated in breast cancer cell lines using MTT and crystal violet assays, flow cytometry, western blot analysis, 3D laser scanning confocal microscopy and transmission electron microscopy. The results showed that GO strongly inhibited cell proliferation, promoted cell apoptosis and cell cycle $G_2$/M arrest, induced the disappearance of cellular microvilli, and enlarged mitochondria. In addition, the protein expression level of AKT, mTOR and p70-S6K decreased in the AKT-mTOR pathway, accompanied by an increase in p-ERK and p-MEK in the MAPK pathway. The results from the present study indicate that GO suppressed breast cancer progression via the MAPK and AKT-mTOR pathways. Taken together, these results provide the basis for a potential therapeutic strategy for breast cancer.

## Introduction

Breast cancer is the most common malignancy in women and remains a major global challenge. Approximately 1.4 million cases occur per year, worldwide (1,2). Surgery, chemotherapy and targeted therapy are the standard treatments for breast cancer. Numerous studies have reported that changes in cell metabolism were associated with transformation and tumor progression, which are associated with electron transport (3,4). In cancer metabolism, electron acceptor deficiency affects NAD+ regeneration from NADH, which indicates that the chemical disposal of excess electrons to synthesize nucleotides could limit proliferation (5). In addition, electron donor and electron acceptor deficiencies lead to an increase in reactive oxygen species (ROS) by affecting ROS detoxification and mitochondrial electron transport chain function, which is consistent with tumor growth (6).

Glyoxal (GO) is the smallest dialdehyde formed in the oxidation-reduction reaction and is associated with electron transfer and metabolism (7,8). A previous study has indicated that GO levels increase in patients with diabetes and reacts with several proteins to form advanced glycation end products via a Maillard-like reaction (9); however, few studies have focused on cancer. In addition, GO has been shown to reduce keratinocyte migration, downregulation of SNAI2 and inhibition of EGF-dependent proliferation (10). Recently, bis(thiosemicarbazones), derived from 1,2-diones, such as GO, have been recognized as potential therapeutic agents against cancer, by suppressing the cell cycle in the human neuroblastoma cell line BE(2)-M17 (11). Meanwhile, in a separate study, the Cu(GTSC) complex, derived from GO, GO-bis(4-methyl-4-phenyl-3-thiosemicarbazonato) copper(II), inhibited tumor growth by 95.0±3.9% in the HCT116 xenograft mouse model (12). Thus, GO could be an important agent for disrupting tumor cell metabolism and a potential anti-cancer target. However, similar to arsenic trioxide, GO has been associated with strong intracellular, digestive and respiratory toxicity, that lead to usage limitations (13,14). Once the balance between the safety and the effects of GO has been achieved, GO might become an effective agent against breast cancer by disrupting cancer metabolism.

The present study aimed to investigate the biofunctions of GO and investigate its molecular mechanisms in breast cancer progression.

## Materials and methods

*Cell lines and culture*. The MDA-MB-231, SUM149 and SUM159 cell lines were used as representative triple-negative breast cancer cell models, while the EMT6 and MCF-7 cell

*Correspondence to:* Professor Li Xianyong, Department of Oncology, Chengdu Fuxing Hospital, 90-1 South Road of Jin Ke, Chengdu, Sichuan 610037, P.R. China
E-mail: lxy1956@yeah.net

*Contributed equally

*Key words:* glyoxal, breast cancer, inhibition, MAPK pathway, AKT/mTOR pathway

lines were used as estrogen receptor-positive breast cancer cell models, and the MCF-10A cell line was used to represent a normal breast cell line. All the cells were purchased from the Shanghai Institutes for Biological Sciences and cultured at 37˚C in a humidified incubator with 5% $CO_2$ in DMEM (HyClone; Cytiva) supplemented with 10% FBS (Natocor) and antibiotics (Sigma-Aldrich; Merck KGaA) (15).

*GO preparations*. GO (Sinopharm Chemical Reagent Co., Ltd.) is an organic compound with the chemical formula OCHCHO, and the Chemical Abstract Service number, 107-22-2. GO was filtered using a 0.22 $\mu$m filter (Millipore Sigma) and stored at 26˚C in the dark.

*MTT assay*. Cell viability was performed using the MTT assay (Sigma-Aldrich; Merck KGaA). The MDA-MB-231, SUM149, SUM159, EMT6, MCF-7 and MCF-10A cell lines ($3x10^3$ cells/well) were seeded in 96-well plates and treated with different concentrations of GO (0.129, 0.258, 0.516, 1.032, 2.065, 4.13 and 8.25 mmol/l for MDA-MB-231, SUM149 and SUM159; and 1.032, 2.065 and 4.13 mmol/l for EMT6, MCF-7 and MCF-10A). After 24 h, 20 $\mu$l 5 mg/ml MTT solution was added to each well and the plates were further incubated at 37˚C for 4 h. Following which, the medium was aspirated, and 200 $\mu$l dimethyl sulfoxide was added to each well. After the purple formazan crystals had dissolved, the absorbance was determined at 492 nm using an INFINITE F50 microplate reader (Tecan Group, Ltd.). According to the MTT data, $IC_{50}$ values were computed by GraphPad Prism (v8.0; GraphPad Prism Software, Inc.). Meanwhile, the $IC_{50}$ for GO was used for 24 h, and the morphology was captured by Nikon TS100 microscope (Nikon Corporation). The results were obtained from three independent experiments.

*Crystal violet assay*. The MDA-MB-231, SUM149, SUM159, EMT6, MCF-7 and MCF-10A cell lines were seeded in 24-well plates, at a density of $1x10^3$ cells/well and incubated for 24 h. The cells were then treated with different concentrations of GO (0.516, 1.032, 2.065, 4.13 and 8.25 mmol/l) continuously for 5 days. After fixation with 4% paraformaldehyde for 30 min at 26˚C, the cells were stained with crystal violet solution for 2 h at 26˚C. The results were obtained from three independent experiments.

*Cell migration assay*. Cell migration ability was performed using a wound-healing assay. Approximately $2x10^4$ cells were seeded into each well of a 6-well plate without serum and a light microscope was used the following day to confirm that each well was coated with cells at ~90% confluence. A 1.0 ml pipette tip was used to remove the cells in the wound-healing region and the plates were washed with PBS three times to remove the displaced cells. The cells were treated with different concentrations of GO (3.550/4.130 mmol/l for MDA-MB-231 and SUM149; 1.437/2.065 mmol/l for SUM159; 1.85/4.13 mmol/l for EMT6; and 1.032/4.13 mmol/l for MCF-7 and MCF-10A). The control cells were incubated with serum-free medium at 37˚C with 5% $CO_2$. At 0, 24 and 48 h, images were captured using a Nikon TS100 microscope (Nikon Corporation), at x40 magnification and the wound was measured using ImageJ software (v1.52a; National Institutes of Health). The experiment was repeated three times.

*3D laser scanning confocal microscope and transmission electron microscope (TEM)*. The MDA-MB-231, SUM149, SUM159 and EMT6 cell lines were treated with different concentrations of GO (3.550, 3.550, 1.437 and 2.22 mmol/l, respectively) for 24 h. For TEM, a total of $1x10^7$ cells were pelleted by centrifugation at 2,683 x g for 5 min at 26˚C, then washed three times with PBS. The cells were then fixed in 2.5% glutaraldehyde at 4˚C for 24 h. Next, the cells were washed with PBS three times and post-fixed in 1% osmium tetroxide for 60 min at 4˚C, encapsulated in 1% agar and stained with uranyl acetate and phosphotungstic acid for 60 min at 4˚C. The cells were then dehydrated in a graded ethanol series and subsequently incubated in propylene oxide for 35 min at 26˚C. The TEM images were captured using a Hitachi TEM system (Hitachi High-Technologies Corporation).

For 3D micro-morphology, the volume and height of the SUM149, MDA-MB-231, SUM159 and EMT6 cell lines were measured using a VK-V150 laser microscopy system (Keyence Corporation). Phase-contrast observations of the cells were performed using an Olympus IX71 microscope (Olympus Corporation). The results were obtained from three independent experiments.

*Western blot analysis*. The protein expression level of ERK, phosphorylated (p)-ERK, MEK, p-MEK, AKT, p-AKT-Ser473, p-AKT-Thr308, mTOR and p70-S6k was measured using western blot analysis in the MDA-MB-231, SUM149 and SUM159 cell lines, which were each treated with the $IC_{50}$ of GO. All cells were lysed in RIPA lysis buffer (cat. no. P0013B; Beyotime Institute of Biotechnology) and then centrifuged at 15,702 x g for 15 min at 4˚C. Protein concentrations were determined using a BCA kit (Beyotime Institute of Biotechnology). A total of 20 $\mu$g protein was separated on 6-10% gels using SDS-PAGE and transferred to PVDF membranes (MilliporeSigma). The membranes were blocked for 1 h at 26˚C with 5% bovine serum albumin containing 0.1% Tween-20. Immunoblotting was performed using the following primary antibodies: ERK (cat. no. 13-6200, 1:1,000), p-ERK (cat. no. 44-680G; 1:500), MEK (cat. no. PA5-116802; 1:500), p-MEK (cat. no. 44-452, 1:1,000), AKT (cat. no. MA191204; 1:1,000), mTOR (cat. no. A301-144A-T; 1:1,000), p70-S6k (cat. no. MA5-36267; 1:1,000) (all Invitrogen; Thermo Fisher Scientific, Inc.) and Tubulin (cat. no. AF1216; 1:1,000; Beyotime Institute of Biotechnology) overnight at 4˚C. The membranes were then washed with 1% TBS-Tween-20 three times and incubated with the corresponding secondary antibodies (cat. no. A0208; goat anti-rabbit; 1:5,000; Beyotime Institute of Biotechnology) at 37˚C for 2 h. The membranes were washed again with TBS, and the proteins were visualized using an enhanced chemiluminescence assay kit (Beyotime Institute of Biotechnology). Images were captured using a Bio-Rad Chemodoc XRS+ system and the Image-lab software (Version 6.0; Bio-Rad Laboratories, Inc.). The test was repeated three times.

*Cell cycle analysis using flow cytometry*. The MDA-MB-231, SUM149 and SUM159 cell lines ($5x10^4$ cells/well) were seeded in 6-well plates and treated with GO ($IC_{50}$: 3.78, 1.85

and 1.60 mmol/l, respectively) for 24 h. Next, the cells were collected and stored in pre-cooled alcohol overnight at 4˚C, then stained with PI (Shanghai Yeasen Biotechnology, Co., Ltd.) for 15 min in the dark at 4˚C. The samples were tested using a Guava EasyCyte Plus flow cytometer (Merck KGaA) and FlowJo VX (Becton-Dickinson and Company) was used to analyze the results. The test was repeated three times.

*Cell apoptosis analysis using flow cytometry*. The MDA-MB-231, SUM149 and SUM159 cell lines ($5x10^4$ cells/well) were seeded in 6-well plates and treated with GO ($IC_{50}$: 3.78, 1.85 and 1.60 mmol/l, respectively) for 24 h. The cells were then collected and stained using the Annexin V/PI kit (Shanghai Yeasen Biotechnology, Co., Ltd.) for 15 min in the dark at 4˚C. The samples were tested using a Guava EasyCyte Plus flow cytometer (Merck KGaA) and FlowJo VX (Becton, Dickinson and Company) was used to analyze the results. The test was repeated three times.

*Statistical analysis*. The data were expressed as the mean ± SD, and unpaired t-tests or repeated measures one-way ANOVA followed by Dunnett's multiple comparisons test were performed for statistical analyses using GraphPad Prism (v8.0; GraphPad Prism Software, Inc.). $P<0.05$ was considered to indicate a statistically significant difference.

## Results

*GO inhibits breast cancer cell proliferation*. MTT and crystal violet assays were used to investigate the biofunctions of GO on cancer cell proliferation in different breast cancer cell lines. The results demonstrated that cell proliferation was inhibited in a concentration-dependent manner. As the GO concentration increased, a greater inhibitory effect was exerted in the breast cancer cell lines. Inhibition rates were up to 78.95±0.05, 88.83±1.35, 87.49±1.11, 88.98±9.90 and 71.77±1.29% for the MDA-MB-231, SUM149, SUM159, EMT6, and MCF-7, respectively ($P<0.05$ compared with cells without GO). However, GO only slightly reduced the proliferation rate in the MCF-10A normal breast cell lines, as the inhibition rate was <38.26%. The $IC_{50}$ values of the MDA-MB-231, SUM149, SUM159, EMT6, MCF-7 and MCF-10A cell lines were 3.78, 1.85, 1.60, 1.29, 2.22, and 4.39 mmol/l, respectively (Fig. 1A). In addition, cellular morphology indicated cell death after treatment with GO for 24 h (Fig. 1B). Furthermore, under the above general tendency, the crystal violet assay showed that cell proliferation was notably suppressed (Fig. 2A).

To further elucidate the mechanisms underlying the action of GO, the protein expression level of the downstream kinases of the MAPK and AKT/mTOR pathways were investigated using western blot analysis. Consistent with the aforementioned results, GO was found to be involved in the regulation of the MEK-ERK and AKT/mTOR pathways. The results indicated that the protein expression level of AKT1 was suppressed in SUM149 and SUM159 group, and the expression level of mTOR and P70-S6K proteins was suppressed in MDA-MB-231, SUM149, and SUM159 cells (Fig. 2B). By contrast, GO also increased p-ERK protein expression in the same cell lines, and p-MEK protein expression increased in MDA-MB-231 and SUM149 cell lines (Fig. 2B). In summary, the results indicated that GO suppressed breast cancer cell proliferation by acting on the MAPK and AKT/mTOR pathways.

*GO inhibits breast cancer cell migration*. To investigate the effect of GO on breast cancer and normal breast cell migration, differences in the wound healing rate in the MDA-MB-231, SUM149, SUM159, EMT6, MCF-7 and MCF-10A cell lines 48 h following GO treatment were observed. The results showed that the relative scratch width of the GO group was significantly wider compared with that in the control group at the 24 and 48 h time points. In the MDA-MB-231 group, the migration inhibition rates were 84.18 and 86.32% at 3.550 and 4.130 mmol/l, respectively. In the SUM149 group, the migration inhibition rates were 81.19 and 82.94% at 3.550 and 4.130 mmol/l, respectively. In the SUM159 group, the migration inhibition rates were 67.65 and 80.00% at 1.437 and 2.065 mmol/l, respectively. In the EMT6 group, the migration inhibition rate was 52.86 and 81.88% at 1.85 and 4.13 mmol/l, respectively. In the MCF-7 cells, the migration inhibition rate was 77.33 and 80.42% at 1.032 and 4.13 mmol/l, respectively. In the MCF-10A normal breast cells, the migration inhibition rate was 44.20 and 44.92% at 1.032 and 4.13 mmol/l, respectively. Under the above general tendency, the data indicated that GO suppressed cell migration in a concentration-dependent manner at both 24 and 48 h ($P<0.05$) (Fig. 3).

*GO induces cellular ultrastructure and changes morphology*. The cellular ultrastructure was observed using TEM. A previous study has indicated that typical morphological features of apoptosis include chromatin condensation, nuclear fragmentation and the disappearance of surface microvilli (16). As shown in Fig. 4, GO treatment for 24 h notably altered the ultrastructure of the mitochondria, nucleus and microvilli. Mitochondria appeared as enlarged organelles. The cellular morphology became irregular and cytoplasmic vacuolization was observed. In addition, rich microvilli, which were around the cells, almost disappeared in the GO group, which is consistent with cell migration inhibition. Chromatin also dissociated and appeared around the edge of the nucleus after treatment with GO. However, the cell membranes remained intact, and chromatin condensation and nuclear fragmentation were not observed in either group.

To improve the understanding into the changes in cellular morphology following GO treatment, a 3D laser scanning confocal microscope was used, which is a valuable tool for obtaining high-resolution images and 3D reconstructions. Treatment with GO for 24 h notably altered cellular morphology, height and volume (Fig. 5A). Compared with that in the control group, the cellular height of the SUM149, MDA-MB-231, SUM159 and EMT6 cell lines decreased 67.22 (4.69±0.23 vs. 1.54±0.29 $\mu$m; $P<0.001$), 74.22 (4.73±0.86 vs. 1.22±0.15 $\mu$m; $P<0.001$), 21.78 (2.96±0.41 vs. 2.32±0.49 $\mu$m; $P<0.05$) and 33.43% (1.98±0.48 vs. 1.32±0.12 $\mu$m; $P<0.05$) (Fig. 5B). In addition, the cellular volume of the SUM149, MDA-MB-231, SUM159 and EMT6 cell lines decreased by 40.29 (797.28±66.43 vs. 476.06±65.02 $\mu m^3$; $P<0.05$), 69.90 (991.09±305.26 vs. 298.30±13.42 $\mu m^3$; $P<0.001$), 72.83

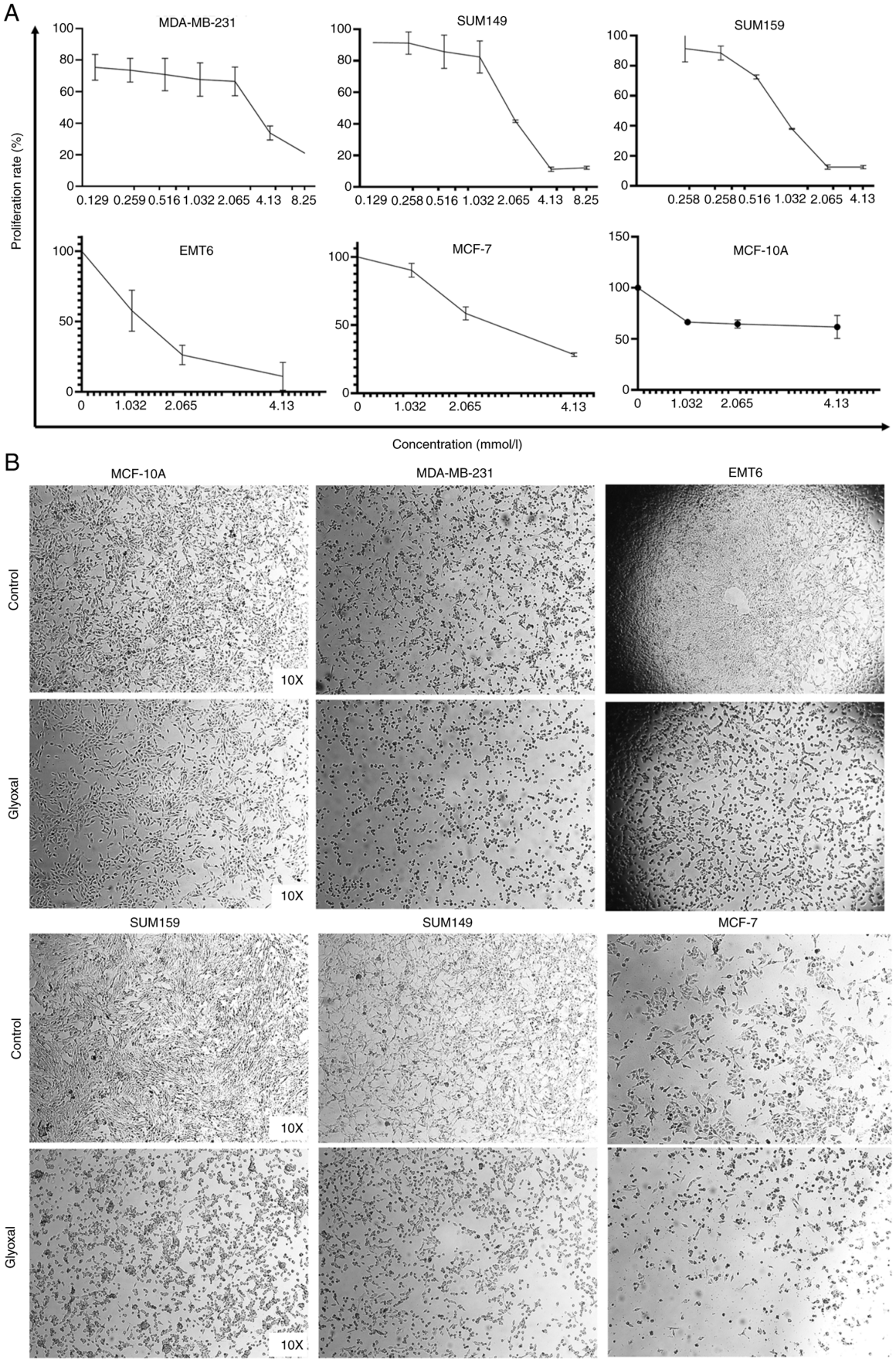


Figure 1. Inhibition ability at different doses of GO was analyzed using the MTT and crystal violet assays in the MDA-MB-231, SUM149, SUM159, EMT6, MCF-7 and MCF-10A cell lines. (A) Under the above general tendency, the results from the MTT assay showed that GO inhibited MDA-MB-231, SUM149, SUM159, EMT6 and MCF-7 cell proliferation in a concentration-dependent manner. GO at 4.13 mmol only notably inhibited the MCF-10A normal breast cell lines. (B) The MDA-MB-231, SUM149, SUM159, EMT6 and MCF-7 cell lines were treated with GO for 24 h and changes in cell morphology and cell death were observed. However, the cell morphology of the MCF-10A cell line was almost normal. GO, glyoxal.

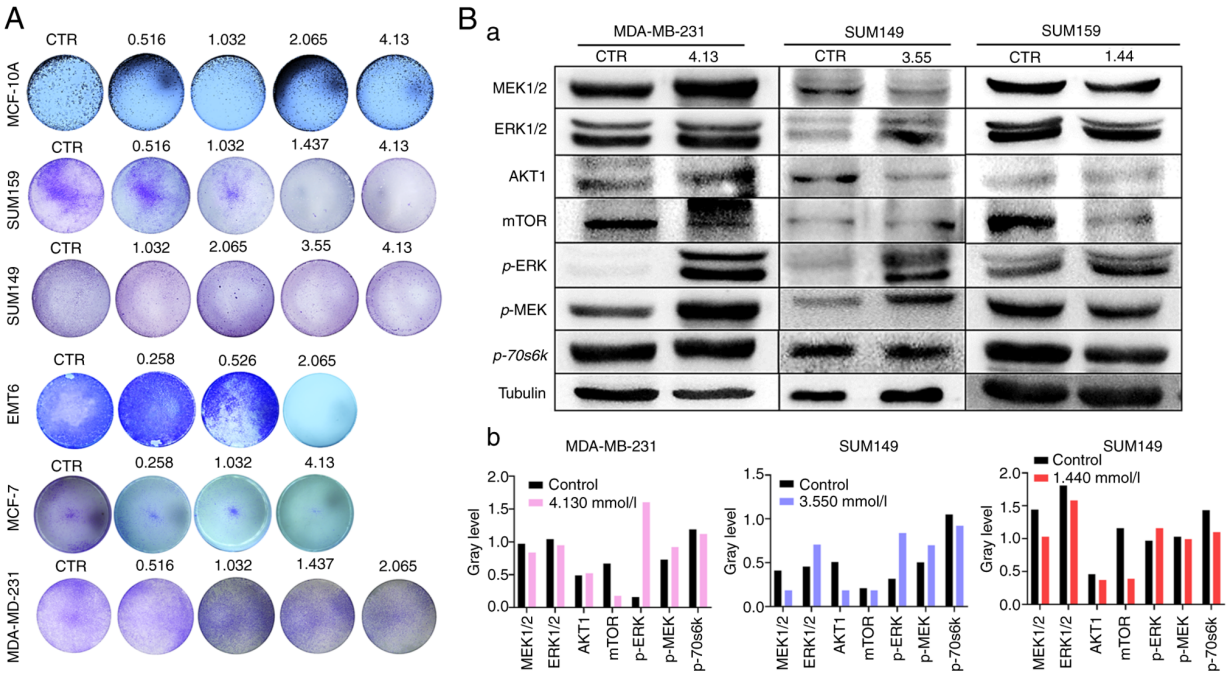


Figure 2. (A) GO notably reduced the colony numbers in the MDA-MB-231, SUM159, MCF-7, MCF-10A and EMT6 cell lines following treatment with different concentrations. (B) The result of Western blot assay. a, TNBC cell lines were treated with GO. The protein expression level of AKT1 decreased in the SUM149 and SUM159 groups, and the expression level of mTOR and P70-S6K proteins decreased in all three cell lines. Meanwhile, p-ERK protein expression increased in all three cell lines, and p-MEK protein expression increased in MDA-MB-231 and SUM149 cell lines. b, Analysis of Western blot bands in each cell line by Image J software (National Institutes of Health, USA). GO, glyoxal; CTR, control; p, phosphorylated.

(982.57±218.70 vs. 266.92±54.35 $\mu m^3$; P<0.001) and 63.29% (1,028.85±203.27 vs. 377.96±15.55 $\mu m^3$; P<0.001) (Fig 5C), respectively. As a result, the cellular morphology was altered, becoming more circular and flatter, and the microvilli on the cell surface also disappeared, which suggested that the cell skeleton was affected and cell apoptosis occurred.

*GO induces cell apoptosis and arrests the cell cycle*. Next, the effects of GO on cell apoptosis and the cell cycle were investigated. As shown in Fig. 6, the proportion of Annexin V (+)/PI (+) apoptotic cells increased significantly following treatment with GO. The percentage of AnnexinV (+)/PI (+) cells in the GO group was 86.97±0.89, 31.8±0.28 and 31.15±3.61% compared with that in the control 5.43±1.57, 15.6±7.21 and 14.65±2.76% for the MDA-MB-231 (P<0.001), SUM149 (P<0.05) and SUM159 (P<0.05) cell lines, respectively (Fig. 6A). In addition, GO arrested the cell cycle. A higher percentage of cells in the $G_1$ phase was accompanied by a decrease in the proportion of cells in the $G_2$/M phase following treatment with GO for 24 h (7.01±1.73 vs. 23.82±2.24% for MDA-MB-231; P=0.014; 10.75±2.33 vs. 83.50±4.10% for SUM149; P=0.002; 42.60±1.41 vs. 67.40±5.94% for SUM159; P=0.029). Thus, these results demonstrated that GO inhibited cell proliferation by arresting the cell cycle in the $G_2$ phase (Fig. 6B).

## Discussion

The morbidity rate of breast cancer has surpassed that of lung cancer so that breast cancer is now the most malignant tumor in the world. Thus, besides chemotherapy, targeted treatment and endocrine treatment, more treatments are required for breast cancer. Cytotoxic agents are no longer the only potential novel anticancer drugs. The 'Warburg effect' suggests that even under oxygen-sufficient conditions, tumor cells still take advantage of glycolysis metabolism, using oxidative phosphorylation, which is associated with the respiratory chain rather than producing ATP (17). Therefore, changes in cancer tissue metabolite levels can have important implications for cell physiology (18), and the majority of previous studies have focused on the role of mitochondria in the regulation of cell proliferation and apoptosis (19-21). During tumor metabolism processes, cytochrome *c* oxidase and succinate dehydrogenase are increased, and the activity of glucose transporters is enhanced. Furthermore, mitochondrial aerobic oxidation is inhibited, disrupting the tricarboxylic acid cycle (22). Zhou *et al* (23) indicated that mitochondrial function plays an important role in the 'bystander effect' mediated by radiation therapy, which relies on the NF-κB/iNOS/COX-2/prostaglandin E2 pathways of mitochondria. In addition, the cell energy metabolism level can be reduced by avicins, which are triterpene compounds that act on the outer mitochondrial membrane by closing voltage-dependent negative ion channels (24).

In addition, tumor cell proliferation is significantly inhibited by dichloroacetic acid, which inhibits mitochondrial pyruvate dehydrogenase kinase and activates potassium channels in all cancer cells, thereby inducing apoptosis (25). In addition, drugs that suppress microvillus development and arrest the cell cycle at the $G_0/G_1$, S or $G_2$ phases, prevent cancer proliferation (19,26-30). In addition, King *et al* (31) summarized and discussed the fact that the activities of succinate dehydrogenase (SDH) and fumaric acid hydratase were associ-

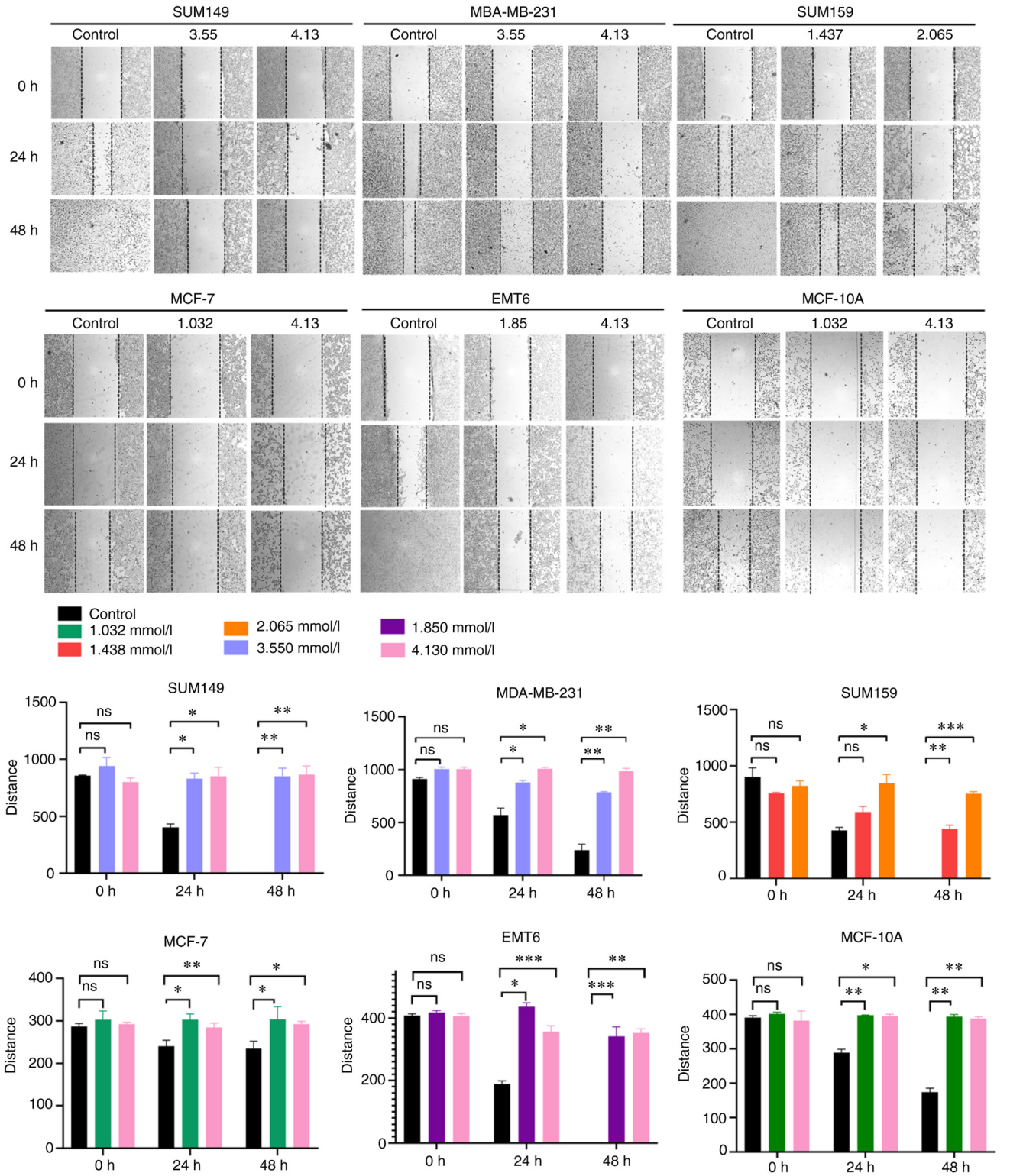


Figure 3. Wound healing assay using the MDA-MB-231, SUM149, SUM159, EMT6, MCF-7 and normal MCF-10A breast cell lines. The migration distance in the glyoxal groups was significantly shorter compared with that in the control group. Images were captured at 0, 24 and 48 h after scratching. $^{*}$P<0.05, $^{**}$P<0.01, $^{***}$P<0.001. Magnification, x40.

ated with mitochondrial dysfunction in malignant tumor cells. Notably, SDH is an important component of the tricarboxylic acid cycle, that plays a key role in the transition of ubiquinone to ubiquinol in the mitochondrial electron transport chain (32). Thus, changes in the electron transfer chain can alter the biological behavior of tumors and interrupting electron transportation in cell metabolism contributes to tumor progression, which is a potential therapeutic target.

Furthermore, metabolic reprogramming is an important hallmark of cancer cell proliferation (33). The preferential use of glycolysis unavoidably generates methylglyoxal (MGO), which is associated with the glycolysis reaction via the spon-

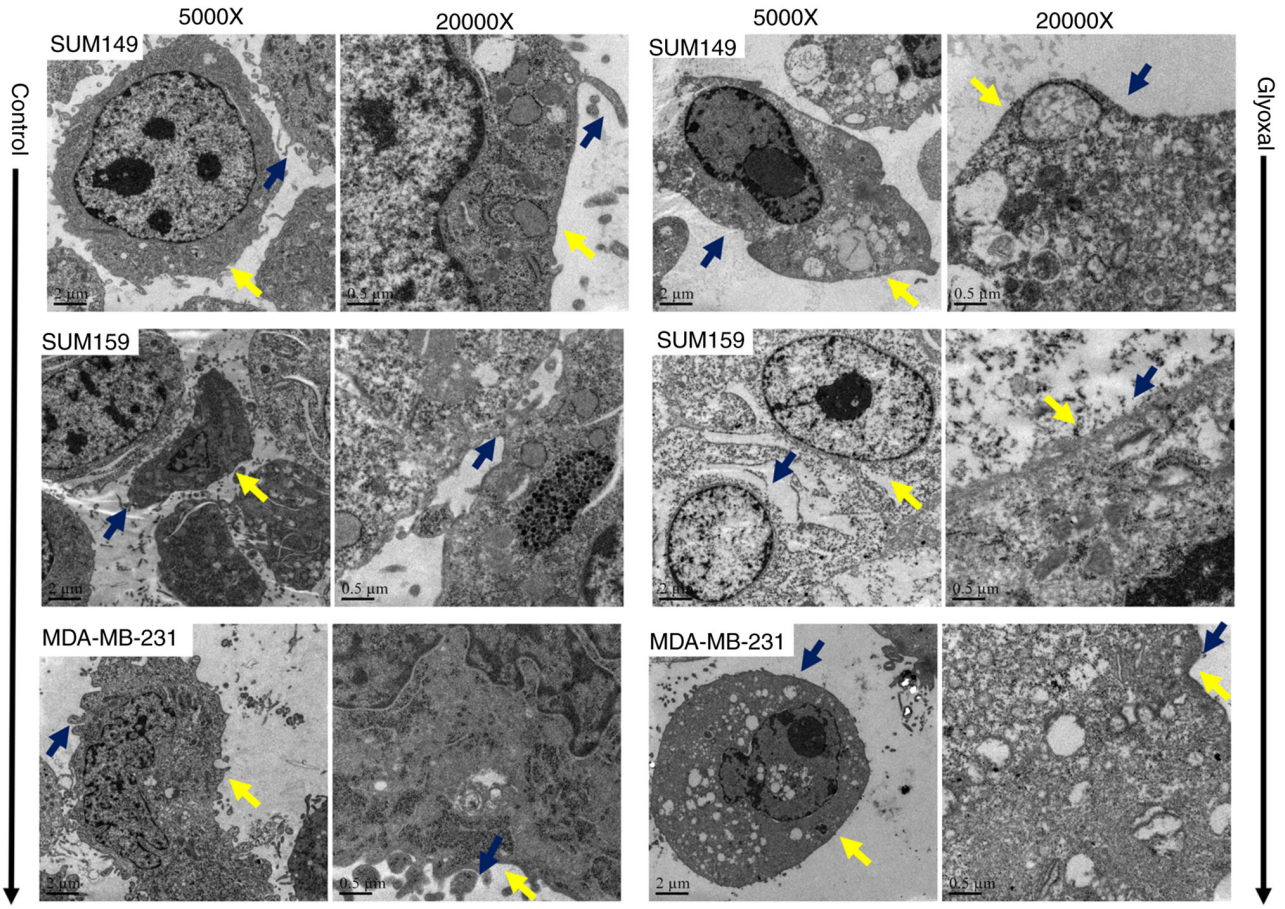


Figure 4. TEM analysis in the SUM149, SUM159 and MDA-MB-231 cell lines. Compared with that in the control group, glyoxal induced cellular surface microvillus disappearance (blue arrow), but the cell membrane remained intact (yellow arrow). Magnification, x5,000 and x20,000.

taneous dephosphorylation of GAP and dihydroxyacetone phosphate (34). A dual role has been previously demonstrated for MGO, which is favorable to neuron viability and excitability at low levels, while high levels are cytotoxic (33). At high concentrations, MGO suppressed breast cancer cell proliferation via glycolysis, but low doses of MGO promoted tumorigenesis even in the same tissue (33,35,36). Accordingly, the expression balance of MGO is more critical than its expression level. By contrast, GO was associated with glycolysis reactions; however, it is the smallest dialdehyde and contains two adjacent reactive carbonyl groups, which form during the oxidation-reduction reaction. These are referred to as reactive electrophilic species and they are more effective than MGO (13,37). Furthermore, GO-induced cytotoxicity and protein carbonylation were more severe than for MGO (37); therefore, GO concentration must be finely adjusted and maintained within a safe range in glycolytic cancer cells. Therefore, GO was selected as the focus of the present study, even though GO can cause mitochondrial toxicity (14,38). In addition, GO plays important roles in cellular responses to energy metabolism and T-cell activation by regulating cell signaling pathways (39,40). In addition, GO impairs the electron transport chain, mitochondrial function and energy metabolism. For example, GO leads to advanced lipoxidation and glycation end products, which are associated with aging and age-related chronic diseases via mitochondrial dysfunction (41).

Therefore, the present study aimed to further investigate the effects and mechanisms of GO stress on breast cancer cells. The results of functional analyses showed that GO treatment notably induced a decrease in cell proliferation, increased cell apoptosis, arrested the cell cycle in $G_2$ phase and altered cellular ultrastructure. The western blot results indicated that GO treatment was involved in the MAPK and mTOR signaling pathways in breast cancer. Taken together, these findings suggest that GO is a potential anti-cancer therapeutic agent that inhibits breast cancer progression by regulating the MAPK and AKT/mTOR signaling pathways. Notably, measuring the increase in cellular levels of p-ERK has been shown to be an indirect indicator of the increase in bioavailable copper that causes cell apoptosis (42,43).

In conclusion, several compounds affect breast cancer cell lines via glycolysis, such as MGO and GO. As GO is the smallest dialdehyde and contains two adjacent reactive carbonyl groups, GO can cause increased cytotoxicity, and protein carbonylation than MGO. However, GO causes severe side-effects and toxicity than MGO; therefore, the concentration of GO must be strictly adjusted to be kept in a safe range. The results from the present study showed that GO could be a potential therapeutic agent for breast cancer; however, additional research is required to gain a more in-depth understanding of its mechanisms.

**Acknowledgements**

Not applicable.

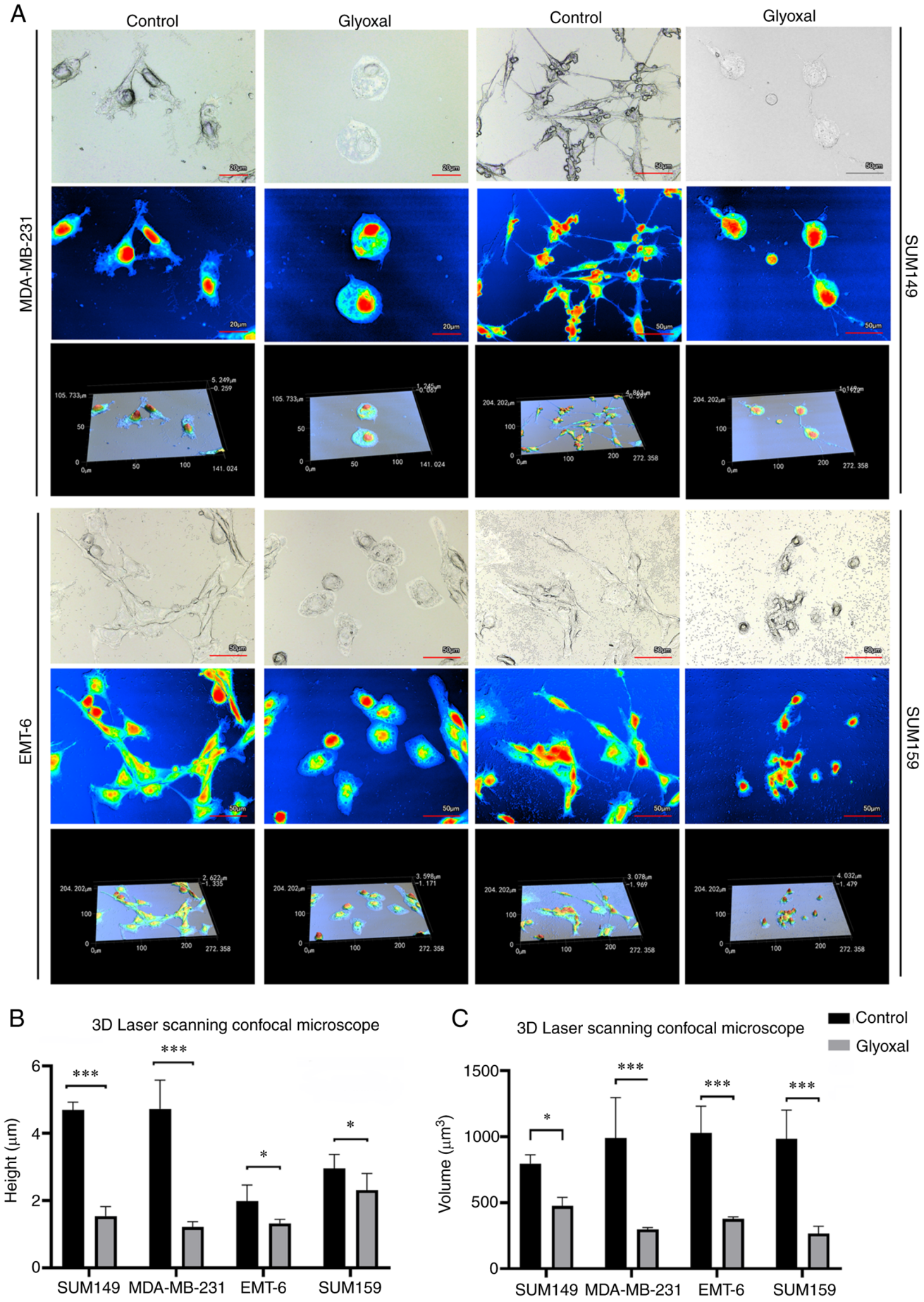


Figure 5. (A) The SUM149, SUM159, MDA-MB-231 and EMT6 cell lines were analyzed using 3D laser scanning confocal microscope. The cell morphology was changed to circular and flat structure following glyoxal treatment. Magnification, x400. Cellular (B) height and (C) volume decreased. $^{*}$P<0.05, $^{***}$P<0.001.

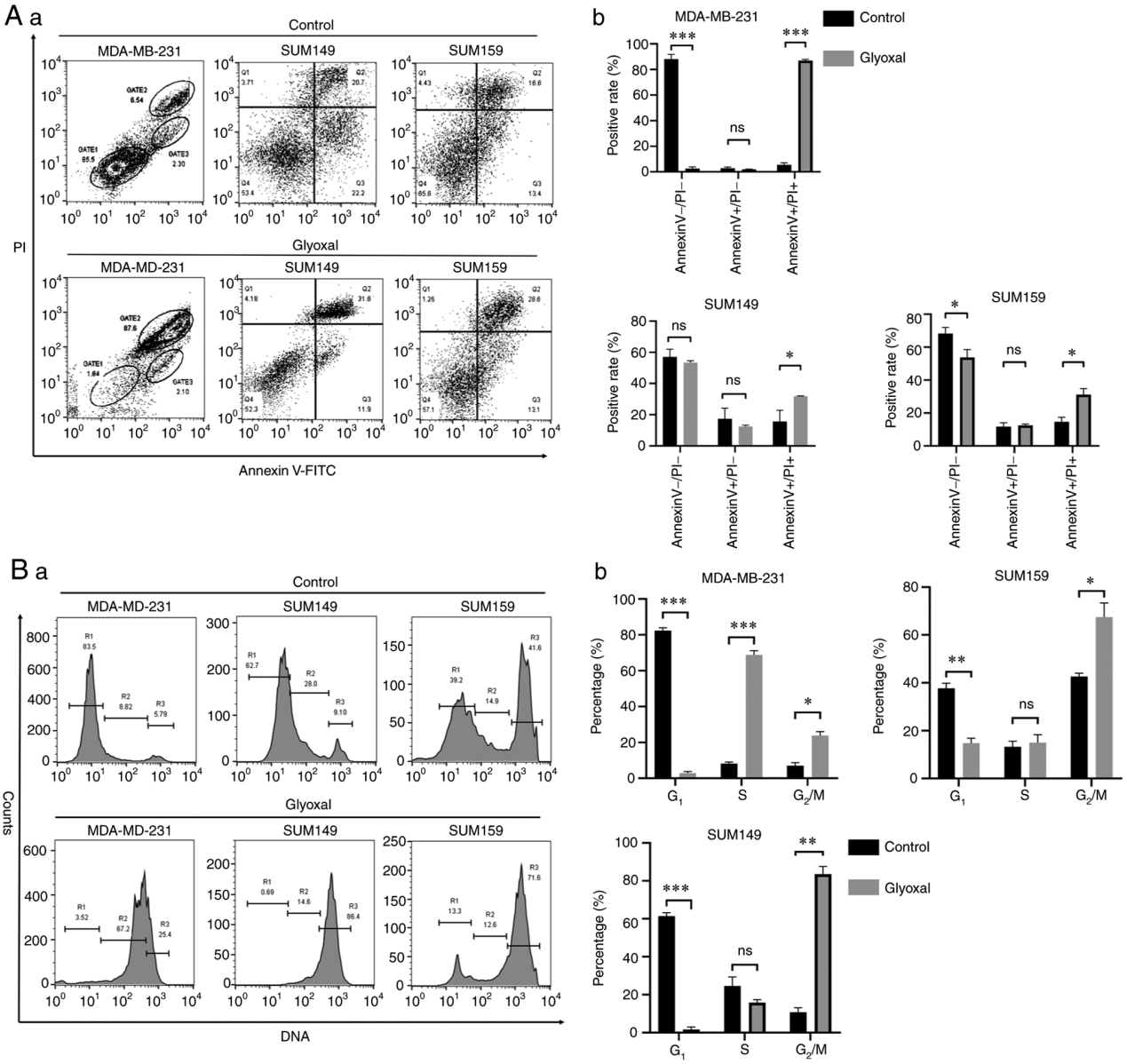


Figure 6. Cell apoptosis and cell cycle was analyzed using flow cytometry. (Aa) Glyoxal increased the positive rate of Annexin $V^+/PI^+$ cells in the MDA-MB-231, SUM149 and SUM159 cell lines and the results were (Ab) statistically analyzed. (Ba) $G_2/M$ phase was arrested in the glyoxal group compared with that in the control group and the results were (Bb) statistically analyzed. $^*P<0.05$, $^{**}P<0.01$, $^{***}P<0.001$.

**Funding**

No funding received.

**Availability of data and materials**

The datasets used and/or analyzed during the current study are available from the corresponding author on reasonable request.

**Authors' contributions**

PR and LY designed the study. GN, LY and LQ contributed to the cell culture and experiments. PR and LX analyzed the data. LX and LY wrote the original paper. PR, LY, GN, LQ and LX confirm the authenticity of all the raw data. All authors have read and approved the manuscript.

**Ethics approval and consent to participate**

Not applicable.

**Patient consent for participation**

Not applicable.

**Competing interests**

The authors declare that they have no competing interests.

**References**

1. Kunkler L: United stand crucial in breast cancer battle. In: China Daily European Weekly. Europe: China Daily, 2011.
2. Calado A, Neves PM, Santos T and Ravasco P: The effect of flaxseed in breast cancer: A literature review. Front Nutr 5: 4, 2018.

3. Vander Heiden MG and DeBerardinis RJ: Understanding the intersections between metabolism and cancer biology. Cell 168: 657-669, 2017.
4. DeBerardinis RJ and Chandel NS: Fundamentals of cancer metabolism. Sci Adv 2: e1600200, 2016.
5. Hung YP, Albeck JG, Tantama M and Yellen G: Imaging cytosolic NADH-NAD(+) redox state with a genetically encoded fluorescent biosensor. Cell Metab 14: 545-554, 2011.
6. Gatenby RA and Gillies RJ: Why do cancers have high aerobic glycolysis? Nat Rev Cancer 4: 891-899, 2004.
7. Haddad M, Perrotte M, Khedher MRB, Demongin C, Lepage A, Fülöp T and Ramassamy C: Methylglyoxal and glyoxal as potential peripheral markers for MCI diagnosis and their effects on the expression of neurotrophic, inflammatory and neurodegenerative factors in neurons and in neuronal derived-extracellular vesicles. Int J Mol Sci 20: 4906, 2019.
8. da Silva G: Hydroxyl radical regeneration in the photochemical oxidation of glyoxal: Kinetics and mechanism of the HC(O)CO + O(2) reaction. Phys Chem Chem Phys 12: 6698-6705, 2010.
9. Banerjee S: Effect of glyoxal modification on a critical arginine residue (Arg-31α) of hemoglobin: Physiological implications of advanced glycated end product an in vitro study. Protein Pept Lett 27: 770-781, 2020.
10. Quan KK, Kusewitt DF and Hudson LG: Glyoxal leads to defective keratinocyte migration and down-regulation of Snai2. J Dermatol Sci 73: 166-169, 2014.
11. Acevedo KM, Hayne DJ, McInnes LE, Noor A, Duncan C, Moujalled D, Volitakis I, Rigopoulos A, Barnham KJ, Villemagne VL, *et al*: Effect of structural modifications to glyoxal-bis(thiosemicarbazonato)copper(II) complexes on cellular copper uptake, copper-mediated ATP7A trafficking, and P-glycoprotein mediated efflux. J Med Chem 61: 711-723, 2018.
12. Palanimuthu D, Shinde SV, Somasundaram K and Samuelson AG: In vitro and in vivo anticancer activity of copper bis(thiosemicarbazone) complexes. J Med Chem 56: 722-734, 2013.
13. Lee C and Park C: Bacterial responses to glyoxal and methylglyoxal: Reactive electrophilic species. Int J Mol Sci 18: 169, 2017.
14. Goudarzi M, Kalantari H and Rezaei M: Glyoxal toxicity in isolated rat liver mitochondria. Hum Exp Toxicol 37: 532-539, 2018.
15. Rangiah K, Tippornwong M, Sangar V, Austin D, Tétreault MP, Rustgi AK, Blair IA and Yu KH: Differential secreted proteome approach in murine model for candidate biomarker discovery in colon cancer. J Proteome Res 8: 5153-5164, 2009.
16. Li X, Li X, Wang J, Ye Z and Li JC: Oridonin up-regulates expression of P21 and induces autophagy and apoptosis in human prostate cancer cells. Int J Biol Sci 8: 901-912, 2012.
17. Warburg O: On respiratory impairment in cancer cells. Science 124: 269-270, 1956.
18. Luengo A, Abbott KL, Davidson SM, Hosios AM, Faubert B, Chan SH, Freinkman E, Zacharias LG, Mathews TP, Clish CB, *et al*: Reactive metabolite production is a targetable liability of glycolytic metabolism in lung cancer. Nat Commun 10: 5604, 2019.
19. Antico Arciuch VG, Elguero ME, Poderoso JJ and Carreras MC: Mitochondrial regulation of cell cycle and proliferation. Antioxid Redox Signal 16: 1150-1180, 2012.
20. Antico Arciuch VG, Galli S, Franco MC, Lam PY, Cadenas E, Carreras MC and Poderoso JJ: Akt1 intramitochondrial cycling is a crucial step in the redox modulation of cell cycle progression. PLoS One 4: e7523, 2009.
21. Gabrielson M, Reizer E, Stål O and Tina E: Mitochondrial regulation of cell cycle progression through SLC25A43. Biochem Biophys Res Commun 469: 1090-1096, 2016.
22. Luo XJ and Cao Y: Research progress on bioenergy metabolic mechanism of cancer*. Prog Biochem Biophy 38: 585-592, 2011.
23. Zhou H, Ivanov VN, Lien YC, Davidson M and Hei TK: Mitochondrial function and nuclear factor-kappaB-mediated signaling in radiation-induced bystander effects. Cancer Res 68: 2233-2240, 2008.
24. Haridas V, Li X, Mizumachi T, Higuchi M, Lemeshko VV, Colombini M and Gutterman JU: Avicins, a novel plant-derived metabolite lowers energy metabolism in tumor cells by targeting the outer mitochondrial membrane. Mitochondrion 7: 234-240, 2007.
25. Bonnet S, Archer SL, Allalunis-Turner J, Haromy A, Beaulieu C, Thompson R, Lee CT, Lopaschuk GD, Puttagunta L, Bonnet S, *et al*: A mitochondria-K+ channel axis is suppressed in cancer and its normalization promotes apoptosis and inhibits cancer growth. Cancer Cell 11: 37-51, 2007.
26. Wu Q, Fan C, Chen T, Liu C, Mei W, Chen S, Wang B, Chen Y and Zheng W: Microwave-assisted synthesis of arene ruthenium(II) complexes that induce S-phase arrest in cancer cells by DNA damage-mediated p53 phosphorylation. Eur J Med Chem 63: 57-63, 2013.
27. Xia L, Shen C, Fu Y, Tian L and Chen M: MGC29506 induces cell cycle arrest and is downregulated in gastric cancer. Cell Immunol 281: 31-36, 2013.
28. Wang L, Cao H, Lu N, Liu L, Wang B, Hu T, Israel DA, Peek RM Jr, Polk DB and Yan F: Berberine inhibits proliferation and down-regulates epidermal growth factor receptor through activation of Cbl in colon tumor cells. PLoS One 8: e56666, 2013.
29. Yu J, Peng Y, Wu LC, Xie Z, Deng Y, Hughes T, He S, Mo X, Chiu M, Wang QE, *et al*: Curcumin down-regulates DNA methyltransferase 1 and plays an anti-leukemic role in acute myeloid leukemia. PLoS One 8: e55934, 2013.
30. Liang Y, Yin D, Hou L, Zheng T, Wang J, Meng X, Lu Z, Song X, Pan S, Jiang H and Liu L: Diphenyl difluoroketone: A potent chemotherapy candidate for human hepatocellular carcinoma. PLoS One 6: e23908, 2011.
31. King A, Selak MA and Gottlieb E: Succinate dehydrogenase and fumarate hydratase: Linking mitochondrial dysfunction and cancer. Oncogene 25: 4675-4682, 2006.
32. Huang S and Millar AH: Succinate dehydrogenase: The complex roles of a simple enzyme. Curr Opin Plant Biol 16: 344-349, 2013.
33. Radu BM, Dumitrescu DI, Mustaciosu CC and Radu M: Dual effect of methylglyoxal on the intracellular $Ca_2^+$ signaling and neurite outgrowth in mouse sensory neurons. Cell Mol Neurobiol 32: 1047-1057, 2012.
34. Phillips SA and Thornalley PJ: The formation of methylglyoxal from triose phosphates. Investigation using a specific assay for methylglyoxal. Eur J Biochem 212: 101-105, 1993.
35. Nokin MJ, Durieux F, Bellier J, Peulen O, Uchida K, Spiegel DA, Cochrane JR, Hutton CA, Castronovo V and Bellahcène A: Hormetic potential of methylglyoxal, a side-product of glycolysis, in switching tumours from growth to death. Sci Rep 7: 11722, 2017.
36. Bellahcène A, Nokin MJ, Castronovo V and Schalkwijk C: Methylglyoxal-derived stress: An emerging biological factor involved in the onset and progression of cancer. Semin Cancer Biol 49: 64-74, 2018.
37. Yang K, Qiang D, Delaney S, Mehta R, Bruce WR and O'Brien PJ: Differences in glyoxal and methylglyoxal metabolism determine cellular susceptibility to protein carbonylation and cytotoxicity. Chem Biol Interact 191: 322-329, 2011.
38. Shangari N, Bruce WR, Poon R and O'Brien PJ: Toxicity of glyoxals-role of oxidative stress, metabolic detoxification and thiamine deficiency. Biochem Soc Trans 31: 1390-1393, 2003.
39. Lee C, Kim I and Park C: Glyoxal detoxification in Escherichia coli K-12 by NADPH dependent aldo-keto reductases. J Microbiol 51: 527-530, 2013.
40. Corbett AJ, Eckle SB, Birkinshaw RW, Liu L, Patel O, Mahony J, Chen Z, Reantragoon R, Meehan B, Cao H, *et al*: T-cell activation by transitory neo-antigens derived from distinct microbial pathways. Nature 509: 361-365, 2014.
41. Moldogazieva NT, Mokhosoev IM, Mel'nikova TI, Porozov YB and Terentiev AA: Oxidative stress and advanced lipoxidation and glycation end products (ALEs and AGEs) in aging and age-related diseases. Oxid Med Cell Longev 2019: 3085756, 2019.
42. Sun Y, Liu WZ, Liu T, Feng X, Yang N and Zhou HF: Signaling pathway of MAPK/ERK in cell proliferation, differentiation, migration, senescence and apoptosis. J Recept Signal Transduct Res 35: 600-604, 2015.
43. Chen X, Lan X, Mo S, Qin J, Li W, Liu P, Han Y and Pi R: p38 and ERK, but not JNK, are involved in copper-induced apoptosis in cultured cerebellar granule neurons. Biochem Biophys Res Commun 379: 944-948, 2009.